ION CHANNELS, RECEPTORS AND TRANSPORTERS

Flow- and voltage-dependent blocking effect of ethosuximide on the inward rectifier K$^+$ (Kir2.1) channel

Chiung-Wei Huang · Chung-Chin Kuo

Abstract Absence seizures are manifestations of abnormal thalamocortical oscillations characterized by spike-and-wave complexes in EEG. Ethosuximide (ETX) is one of the principal medications against absence seizures. We investigate the effect of ETX on the Kir2.1 channel, a prototypical inward rectifier K$^+$ channel possibly playing an important role in the setting of neuronal membrane potential. We demonstrate that the outward currents of Kir2.1 channels are significantly inhibited by intracellular ETX. We further show that the movement of neutral molecule ETX in the Kir2.1 channel is accompanied by ~1.2 K$^+$, giving rise to the vivid voltage dependence of ETX unbinding rate. Moreover, the apparent affinity (K_d) of ETX in the channels are decreased by single-point mutations involving M183, E224, and S165, and especially by double mutations involving T141/S165, which always also disrupt the flux-coupling feature of ETX block. Molecular dynamics simulation demonstrates narrowing of the pore at ~D172 by binding of ETX to S165 or T141. ETX block of the Kir2.1 channels may cause a modest but critical depolarization of the relevant neurons, decreasing available T-type Ca^{2+} channels and consequently lessening pathological thalamocortical burst discharges.

Keywords Inward rectifier K$^+$ channels · Ethosuximide · Absence seizure · Flow-dependent block · Voltage-dependent block

C.-W. Huang · C.-C. Kuo (✉)
Department of Physiology, National Taiwan University College of Medicine, No. 1, Jen–Ai Road, 1st Section, Taipei 100, Taiwan
e-mail: chungchinkuo@ntu.edu.tw

C.-C. Kuo
Department of Neurology, National Taiwan University Hospital, Taipei, Taiwan

Introduction

Absence seizures are characterized by abnormal thalamocortical oscillations promoted by the burst mode of thalamic discharges [6, 13, 19, 33]. Ethosuximide (ETX, 2-ethyl-2-methylsuccinimide) is one of the principal medications against absence seizures [11, 33, 45]. There are also studies suggesting that ETX has the potential for the treatment of some major comorbidities of seizures, including anxiety- and depression-like behavioral symptoms [2, 11, 37, 39, 45]. Previous studies on isolated thalamic and cortical neurons demonstrated reduction of the T-type Ca^{2+} currents by therapeutic concentrations (0.5~1.0 mM) of ETX [4, 24, 36]. Because the T-type Ca^{2+} channel is an essential element for the generation of thalamic burst discharges, which predominates the cellular activity pattern relevant to absence seizures [22], the inhibitory effect on T-type Ca^{2+} currents has been presumed to be the mechanism underlying anti-absence effect of ETX. However, there are contradictory reports which fail to show a direct inhibitory effect of ETX on T-type Ca^{2+} currents [22, 38, 44]. The origin of the anti-absence effect of ETX has thus remained unsettled [5]. In this regard, ETX has been shown to decrease persistent Na$^+$ and possibly also Ca^{2+}-activated K$^+$ currents in thalamocortical relay and thalamic reticular neurons [5, 12, 26]. It would be desirable to explore whether ETX has an effect on the other channels which may also play an important role in the generation of thalamocortical burst discharges and therefore absence seizures.

Inward rectifier K$^+$ channels (Kir channels) are widely expressed in neurons and glial cells in the central nervous system [5, 12, 16, 21, 26, 28, 34]. Kir channels may play an important role in setting membrane potential and controlling neuronal discharge patterns [15, 30, 49]. Kir channels are also important in the regulation of extracellular K$^+$ concentration which could have a significant impact on neuronal excitability and synaptic transmission [15, 30, 49]. Moreover, Kir

channels have been implicated in the generation of seizure activities [29, 30, 42, 48]. Astrocytic Kir 4.1 channels in amygdala may play an important role in pilocarpine-induced temporal lobe epilepsy, and the Kir 6.2 channels in substantia nigra pars reticulata (SNr) could be involved in hypoxia-induced seizures [42, 48]. Three millimolar ETX (but not valproic acid (VPA)) was shown to inhibit ~50 % of the inward currents in the G protein-activated inwardly rectifying K^+ (GIRK) channels at −70 mV [23]. Of note, the strongest inward rectifying K^+ channel (Kir2.1 channel) is present in the anterior, posterior, and reticular thalamic nuclei [28, 34], which are involved in many critical cognitive processes. In cocultures of thalamic and cortical neurons, Kir2.1-overexpressing neurons tend to have slightly more hyperpolarized membrane potentials and smaller membrane resistances [49]. Here, we show that intracellular ETX blocks the outward currents more effectively than the inward currents through the Kir2.1 channel. The site responsible for this inward rectifying block is located at electrical distance (δ) ~0.5 from the intracellular milieu, most likely at S165/T141 or the external end of the flux-coupling segment in the bundle-crossing region of the pore. It is plausible that ETX may decrease Kir2.1 currents to increase the tendency of a more depolarized membrane potential, leading to a decreased tendency of thalamocortical burst discharges and therefore ameliorating absence seizures.

Materials and methods

Kir2.1 channel expression in *Xenopus* oocytes

This part of the methods is basically the same as that described in the previous study [17, 18]. Mutant channel complementary DNAs (cDNAs) were made using the Quick Change site-directed mutagenesis kit (Stratagene, LA Jolla, CA, USA). Each mutant DNA of Kir2.1 channels was confirmed by automatic DNA sequencer (Applied Biosystems, 3730Xl DNA, Analyzer Foster, CA, USA). These plasmids DNA of Kir2.1 channel were linearized by digestion with the NotI restricted enzyme as described previously [17, 18]. Complementary RNA (cRNA) was made from purified linearized cDNA with in vitro T7 polymerase transcription reactions (mMESSAGE mMACHINE, Ambio, Austin, TX, USA). *Xenopus* oocytes (stages V and VI) were isolated by partial ovariectomy from frogs anesthetized with 0.1 % tricaine, defolliculated using 2 % collagenase and then maintained at 18 °C in ND 96 solution which contains the following: 96 mM NaCl, 5 mM HEPES, 2 mM KCl, 1.8 mM $MgCl_2$, 1.0 mM $CaCl_2$, as well as 20 μg/ml gentamicin, titrate to pH 7.6 by NaOH. Oocytes were pressure microinjected with Kir2.1 cRNA 24 h after defolliculation and were used for electrophysiological recordings (excise inside-out giant patch

clamp) within 1–5 days. All animal experiments were performed in accordance with animal welfare guidelines for the Care and Use of Laboratory Animals promulgated by the National Institutes of Health (NIH) and were approved by the Institutional Animal Care and Use Committee (IACUC) of National Taiwan University College of Medicine (approval and permit number 95–2320).

Electrophysiological measurements

Macroscopic currents were recorded from excise inside-out giant patches from *Xenopus* oocytes expressing wild-type (WT) or mutant Kir2.1 channels with the pClamp 6.0 software and an Axopatch 200A amplifier (Axon Instruments, Inc., Sunnyvale, CA, USA) [17, 18]. Data were filtered at 1~2 kHz and digitized at 1~10 kHz (Digidata 1200A; Axon Instruments, Inc., Sunnyvale, CA, USA). The pipettes were pulled from borosilicate glass. The pipette resistance was 200~400 kΩ when filled with extracellular solutions. Unless otherwise specified, the extracellular and intracellular solutions both contained (in mM) 68 KCl, 4 KOH, 8 K_2HPO_4, 2 KH_2PO_4, and 5 K_2EDTA, pH 7.4 (the "100 mM K^+ solution") [17, 18]. The intracellular solutions also contained 25 μM L-α-phosphatidylinositol-4, 5-bisphosphate (PIP_2), 0.5~100 mM ETX, 0.5~1.0 mM VPA (both from Sigma Chemical Co., St. Louis, MO, USA), 0.5~10 mM succinimide (SUX) (from the Kanto Chemical Co., Kagaku, Japan), and 10 nM spermine (SPM) (from Sigma Chemical Co., St. Louis, MO, USA). For the experiments in 4 mM external K^+, the intracellular solution was not changed, but the extracellular solution contained (in mM) 2 KCl, 0.8 K_2HPO_4, 0.2 KH_2PO_4, and 0.5 EDTA, titrated to pH 7.4 with KOH (the "4 mM K^+ solution"). For the experiments in symmetrical 10 mM K^+, both intracellular and extracellular solutions contained (in mM) 4.6 KCl, 0.9 KOH, 2 K_2HPO_4, 0.5 KH_2PO_4, and 1 EDTA, titrated to pH 7.4 with KOH (the "10 mM K^+ solution"). For the experiments in symmetrical 300 mM K^+, the extracellular and intracellular solutions both contained (in mM) 268 KCl, 4 KOH, 8 K_2HPO_4, 2 KH_2PO_4, and 5 K_2EDTA (the "300 mM K^+ solution"), pH 7.4. The excised inside-out giant patch was moved in front of an array of square glass emitting the intracellular solution and thus subject to continuous perfusion of the intracellular solution for at least 5 min to wash out potential intracellular endogenous blockers before actual experiments were carried out.

Data analysis

The susceptibility of mutant and WT Kir2.1 channels to internal ETX was examined based on apparent K_d values. Briefly, this part of the methods is same as that described in the previous study [17, 18]. The dose–response relationships of the ETX block of Kir2.1 channel were fitted using the

modified Hill's equation (Eq. 1). We found that the data of steady-state ETX block could be reasonably fitted with the equation at membrane potentials more positive than approximately −30 mV (in symmetrical 100 mM K$^+$) or more positive than approximately −110 mV (in 4 mM external/100 mM internal K$^+$).

$$f = \frac{1}{1 + \frac{[ETX]}{Kd}} \qquad (1)$$

In Eq. 1, K_d is the apparent dissociation constant of ETX, [ETX] is the concentration of ETX, and f is the ratio between the steady-state current amplitude in ETX and that in control (relative current). All data are expressed as mean ±SEM.

Homology modeling of the Kir2.1 channels

This part of the methods is basically the same as that described in the previous study [17, 18]. Homology models of the mouse Kir2.1 channel were built based on the coordinates from the X-ray crystal structure of the mouse Kir2.1 (PDB ID: 1U4F) and chicken Kir 2.2 channel (PDB ID: 3SPI) [14, 32, 43]. The aligned sequences were presented to the Discovery Studio v2.5 program (DS v2.5) (Accelrys Inc., San Diego, CA, USA) to generate the secondary structure and relative positions of the chosen residues of the Kir2.1 model [17, 18, 35].

Molecular dynamics simulation of the Kir2.1 channels

Molecular dynamics simulation of the Kir2.1 channels was also performed using the Chemistry at HARvard Molecular Mechanics (CHARMm) force field [18, 27, 40] and Discovery Studio v2.5 Client programs (Accelrys Inc., San Diego, CA, USA) [17, 18, 35]. The counter ions were added to ensure that the overall net charge on the simulation system was zero. The simulation system provides an appropriate environment for the interaction site water model [18]. The water molecules and K$^+$ ions were free to move during the minimization, heating, equilibration, and production process. The Leapfrog Verlet procedure was used to integrate the equation of motion. The Van der Waal's force was modeled with a cutoff value of 10 Å. Berendsen coupling was applied for the simulation parameters to maintain a constant temperature of 300 °K and a constant pressure of 1 bar [1]. In the presence of ~40 water molecules, 7 K$^+$ ions and/or 1 ETX or SUX or VPA or SPM molecule were applied to the cavity region between residues 141 and 165 of WT, S165L, T141A, and T141A/S165L single and double mutant channels to select the one with the lowest potential energy for equilibration from ~10 candidate models.

Results

Inhibition of WT Kir2.1 currents by internal ETX in symmetrical 100 mM K$^+$

We first investigated the effect of ETX on WT Kir2.1 channels. Figure 1a shows evident inhibition of macroscopic WT Kir2.1 currents in symmetrical 100 mM K$^+$ by therapeutic concentrations (0.5 and 1.0 mM) of intracellular ETX. Moreover, the outward currents show accelerated decay in an ETX dose-dependent fashion. The K_d of ETX in symmetrical 100 mM K$^+$ does not change as sharply around 0 mV (the reversal potential, or E_{Rev} of K$^+$, Fig. 1b, c) as the cases of, for example, the strongly inward rectifying block by intracellular spermine (SPM) [17]. The ratio between K_d values at −30 and +30 mV is only ~20, much smaller than that reported for SPM (~102,000 [17]). We also tried to separate the voltage dependence (the dashed line in Fig. 1c) from the flow dependence by the inward rectification index (IR index [17]) which is defined by the ratio
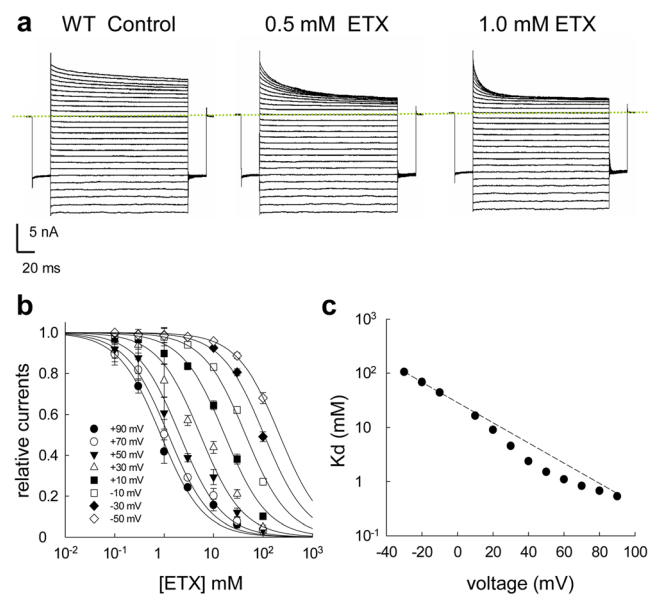
Fig. 1 Inhibition of wild-type (WT) Kir2.1 currents by different concentrations of internal ethosuximide (ETX) in symmetrical 100 mM K$^+$. **a** Sample sweeps demonstrating inhibition of WT Kir2.1 currents in the same patch by 0.5 and 1.0 mM internal ETX in symmetrical 100 mM K$^+$. The patch was first hyperpolarized from the 0 mV holding potential to −100 mV for 20 ms and then stepped to test voltages between −150 and +100 mV for 150 ms in 10-mV increment. The *dotted lines* indicate the zero current level. **b** The relative currents are defined by the ratio between the steady-state currents in ETX and in control and are plotted against ETX concentration (*n*=5–8). The *lines* are fits with Eq. 1 to obtain the apparent dissociation constant (K_d) of ETX. **c** The K_d from **b** is plotted against voltage in a semilogarithmic scale. The K_d values at −30 to −10 mV are fitted with a function $K_{d(V)}=K_{d(0)}\exp(−Z\delta V/25 \text{ mV})$, with $K_{d(0)}$=27.2 mM and $Z\delta$=1.08 (the *dashed line*), where $Z\delta$ is the product of the functional charges on the blocker and the electric distance of the blocking site from the inside, and V is membrane voltage in millivolts (mV)

between the K_d predicted by the dashed line and the actually measured value at +30 mV. The IR index is only ~1.7 for ETX block in the WT Kir2.1 channel (Fig. 1c), in contrast to ~1,200 for SPM [17].

Inhibition of WT Kir2.1 currents by internal ETX in 4 mM external and 100 mM internal K+

We further examined the effect of the internal ETX in 4 mM external and 100 mM internal K+ (for a more physiological E_{Rev} of approximately −80 mV) (Fig. 2a–c). The K_d in asymmetrical (4 mM/100 mM) K+ changes even less sharply in the vicinity of the reversal potential −80 mV. Moreover, it is noted that the K_d values in 4 mM/100 mM K+ are smaller than that in symmetrical 100 mM K+, implying stronger blocking effect of internal ETX with lower concentrations of external K+. This finding indicates that internal ETX blocks the channel at a point where it may interact with external K+. In other words, ETX should block the Kir2.1 channel in the pore.

Two components of internal ETX unblock in WT Kir2.1 channel

If ETX inhibits the Kir2.1 channel as a pore blocker, it is intriguing how the blocking constant (K_d) should be apparently voltage-dependent, because ETX is mostly uncharged in physiological conditions (pH$_i$=7.4). We therefore explored the kinetics of ETX binding to and unbinding from the WT Kir2.1 channel in more detail. We found a "slow tail" when the patch was repolarized from +100 to −100 mV pulse only in the presence but not in the absence of internal ETX (Fig. 3a). The slow tail thus is most likely ascribable to the slow unbinding of ETX from its pore-blocking site [17, 18]. Consistently, the slow tail shows the same decay time constant irrespective of the length at the +100 mV pulse. The amplitude of the slow tail, however, becomes larger with lengthening of the +100 mV pulse before reaching a saturating level. The development of the slow tail therefore may signal the course of ETX binding to this slow unbinding site at the preceding pulse at +100 mV and indeed shares a very similar time course of the decay of the macroscopic outward currents at +100 mV (Fig. 3b). A closer look at the saturating amplitude of slow tail in Fig. 3a, however, reveals that it is always ~40 % (the fast phase is always ~60 %, and thus, the fast phase/slow phase amplitude ratio is ~1.5) of the total inward current irrespective in either 1.0 or 4.0 mM ETX (Fig. 3c). This finding suggests that the blocking ETX may be "pushed" by the outward or inward K+ flux to assume a more external or more internal blocking position and consequently a different blocking effect on K+ currents (see Discussion for more details). The ETX blocking site(s) thus should be located in a flux-coupling region of the pore.
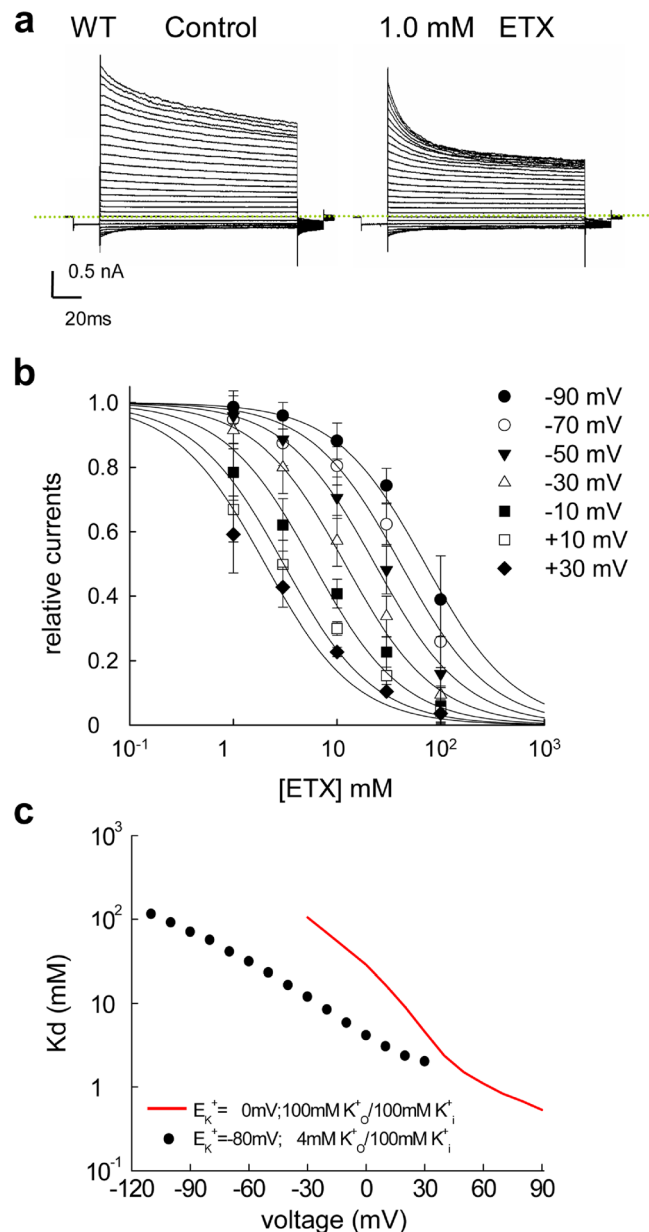

Fig. 2 Inhibition of WT Kir2.1 currents by internal ETX in external 4 mM/internal 100 mM K+. **a** Sample sweeps demonstrating inhibition of WT Kir2.1 currents by internal ETX in the same patch in external 4 mM/internal 100 mM K+. The holding potential is −80 mV rather than 0 mV; otherwise, the pulse protocol is the same as that in Fig. 1a. The *dotted lines* indicate the zero current level. **b** The apparent K_d is obtained by the same way as that in Fig. 1b (n=5–8). **c** The K_d–voltage relationship in external 4 mM/internal 100 mM K+ (the same approach as that in Fig. 1c). The K_d values between −110 and −90 mV are fitted with $K_{d(0)}$=6.3 mM and $Z\delta$=0.67. The K_d–voltage relationship in symmetrical 100 mM K+ in Fig. 1c (*red line*) are replotted here for comparison

Strong voltage dependence in the unbinding kinetics but negligible voltage dependence in the binding kinetics of internal ETX

The binding rate of ETX to this flow-dependent blocking site is barely voltage-dependent ($Z\delta$ ~0.06, Fig. 3d, e). In contrast,
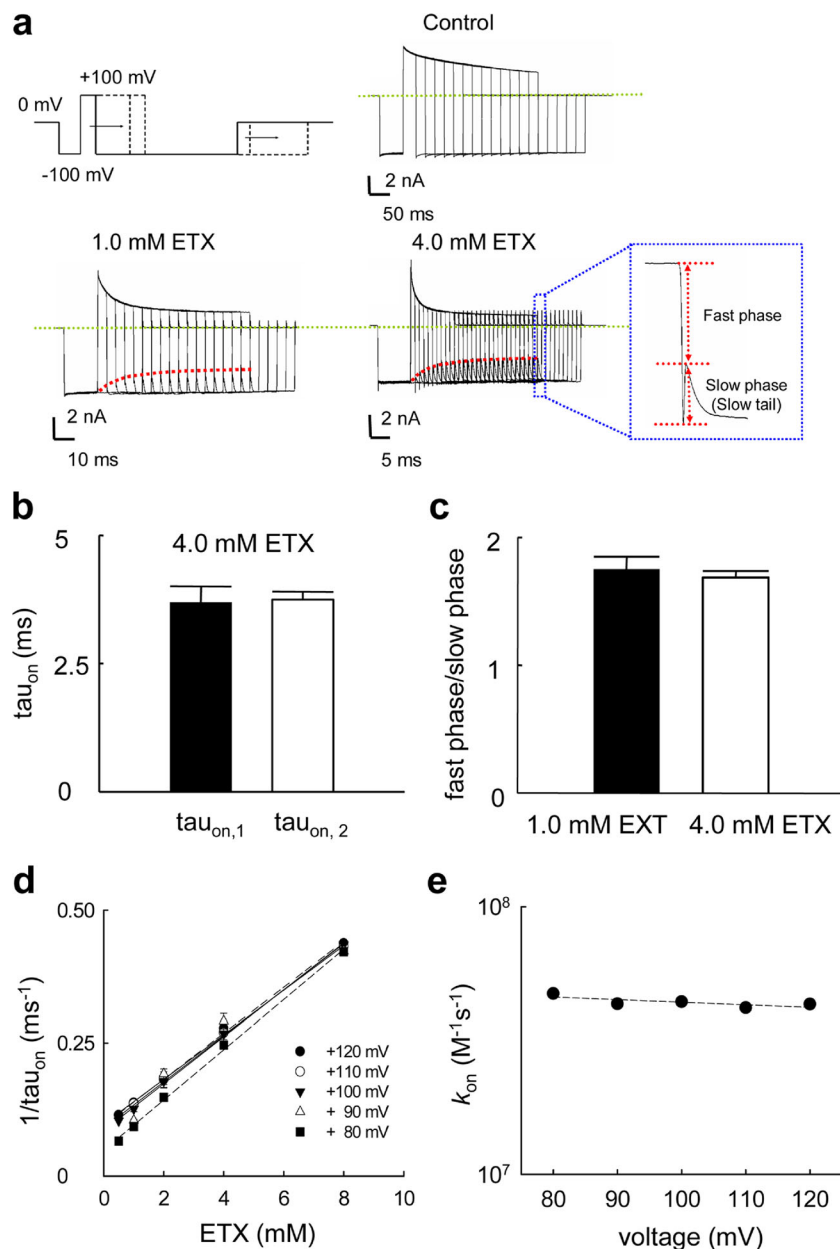
Fig. 3 The slow component of internal ETX unblock in WT Kir2.1 channel. **a** The patch was held at 0 mV and pulsed twice to −100 mV. The intervening depolarization gap between the two pulses was set at +100 mV and lengthened by 10 ms between each sweep. The *dotted lines* indicate zero current level. Note that the slow tail gets larger with lengthening of the +100 mV pulse (until a plateau is reached, *red dotted lines*). Also the development of the slow tail is faster in 4.0 mM than in 1.0 mM ETX (the monoexponential fits to the *red dotted lines* show time constants of ~7.9 and ~3.8 ms for internal 1.0 and 4.0 mM ETX, respectively) (see the *inset figure* for the detailed illustration of the slow phase (slow tail) and the fast phase. **b** Cumulative results were obtained from four patches with the same protocol described in **a**. The very similar

$tau_{on,1}$ and $tau_{on,2}$ are the time constants of the development of the slow tails and the decay of the macroscopic outward currents in 4.0 mM ETX, respectively. **c** The ratio between the amplitude of the fast and slow phases of the inward currents upon stepping to −100 mV from +100 mV in **a** is almost identical in 1.0 and 4.0 mM ETX (n=5–7). **d** The reciprocals of the time constants for the development of the slow tail in **a** ($1/tau_{on}$ or the on rates) are plotted against the ETX concentration (with the intervening depolarization gaps set between +80 and +120 mV and linear fits in *dashed lines*, n=5–7). **e** The slope in **d** is plotted against voltage and fitted with a *regression line* of the form $k_{on}=5.5\times10^7 \exp(0.06\,V/25\,mV)/M/s$, where V is the intervening depolarization voltage in millivolts (mV)

the unbinding rate is strongly voltage-dependent ($Z\delta$ ~0.58, Fig. 4a, b). Because the voltage dependence of on and off rates is obtained with preponderant outward (+80~+120 mV) and inward currents (−20 to −100 mV), respectively, the foregoing

voltage dependence should be close to the "true" voltage dependence devoid of flux-coupling effect. In view of the electroneutral nature of the ETX molecule, the true voltage dependence most likely arises from charged particles
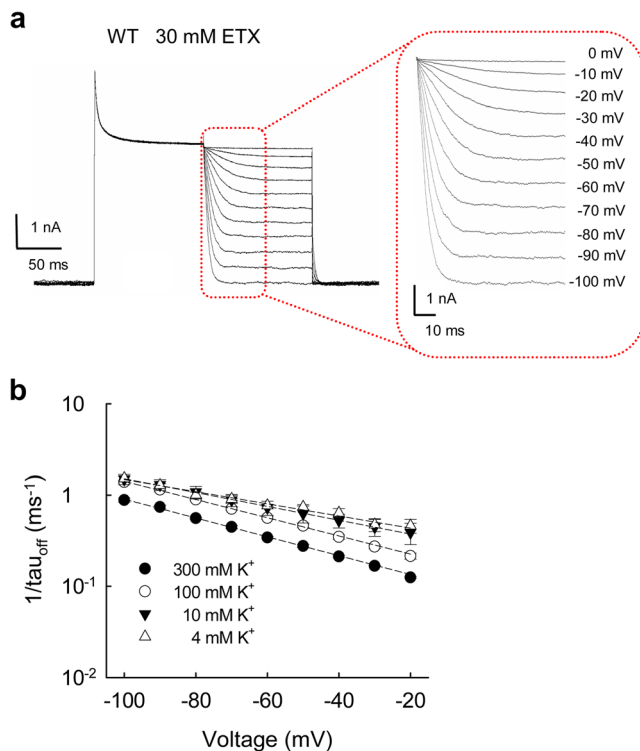
Fig. 4 Voltage dependence of ETX unblocking kinetics in the WT Kir2.1 channels. **a** The voltage across the patch membrane was stepped from the holding potential −100 to +100 mV for ~50 ms and then stepped to different test voltages between −100 and 0 mV for ~100 ms in 10-mV increment in symmetrical 100 mM K$^+$ 30 mM internal ETX. Note the faster decay of the slow tail (the faster unbinding rates of ETX) at more negative potentials. The *dotted lines* indicate the zero current level. **b** The inverses of the time constants of the slow tail currents in part **a** are plotted against membrane potential (n=5–7). The off rates (1/tau$_{off}$) are fitted with a *regression line* of the form 0.14 exp (−0.58 V/25)/ms in 100 mM K$^+$. The off rates revealed by similar experiments are 0.08 exp (−0.58 V/25)/ms, 0.26 exp (−0.43 V/25)/ms, and 0.32 exp (−0.38 V/25)/ms in symmetrical 300, 10, and 4 mM K$^+$, respectively

accompanying the moving and blocking ETX, presumably permeating K$^+$ ions in this case. We therefore examined the ETX slow off-tail currents between −20 and −100 mV also in symmetrical 4, 10, and 300 mM K$^+$. The unbinding kinetics of ETX in symmetrical 4 and 10 mM K$^+$ are faster but less voltage-dependent than that in symmetrical 100 mM K$^+$. The Zδ value decreases from ~0.58 in symmetrical 300 or 100 mM K$^+$ to 0.43 in 10 mM K$^+$, and 0.38 in 4 mM K$^+$ (Fig. 4b). The reasonable linear correlation in all the four sets of data (4, 10, 100, and 300 mM K$^+$) and the tendency, as well as saturation of the voltage dependence change with K$^+$ concentrations would argue against significant artifact caused by the very different ionic milieu beyond the physiological range. These findings therefore lend a strong support for the view that the movement of ETX is coupled by permeating K$^+$ ions. The faster unbinding kinetics in lower ambient K$^+$ concentration, on the other hand, signal K$^+$ occupancy at the (internal) pore mouth and consequent

retardation of the inward exit of ETX with inward K$^+$ flux (see Discussion for details).

Decrease of voltage and flow dependence of ETX block in the E224G and M183N mutant channels

We have demonstrated that internal SPM block of the Kir2.1 channel is similarly composed of a voltage-independent binding and a voltage-dependent unbinding process. Also, SPM unbinding from the Kir2.1 channel pore is composed of a fast and a slow phase [17]. We have further located the flux-coupling segment of the Kir2.1 channel pore to the bundle crossing region, which internal SPM must traverse to reach its blocking site at D172/S165 [17]. In view of the apparent similarity between ETX and SPM blocking the Kir2.1 channel pore, we explored the effect of ETX on the M183N and E224G mutant channels (Fig. 5), two point mutations directly (M183N) or allosterically (E224G) causing narrowing of the pore at the bundle-crossing region [17]. The ETX K_d values are much less voltage-dependent and show no abrupt change around the reversal potential in the E224G and M183N mutant channels with IR indices of 0.9 and 1.0, respectively (Fig. 5c). These findings support that internal ETX, just like SPM, also has to go through the flux-coupling bundle-crossing region of the pore to reach the final blocking site.

Decrease of ETX blocking effect in the S165L but not D172N mutant channels

It has been shown that internal SPM blocks the Kir2.1 channel pore at a site at the external end of the flux-coupling bundle-crossing region, probably composed of D172 and demarcated externally by S165 [9, 17]. We found that, in sharp contrast to the case of SPM block, D172N mutation has only a negligible effect on ETX block (Fig. 6; see also Discussion and Fig. 8). On the other hand, S165L mutation, which has a less profound effect on SPM block of inward currents but markedly increases the chance of outward exit of SPM with outward currents [17], significantly decreases the blocking effect of ETX especially at positive voltages (Fig. 6c). We also examined the effect of the other substitutions (A, C, G, P, K, and R) for S165 and got four more mutant channels (S165A, S165C, S165G, and S165P) showing enough currents for analysis (Fig. S1). The findings are qualitatively similar among these different S165 mutant channels, which show markedly decreased or essentially negligible changes around the reversal potential (0 mV) in the ETX K_d–V_m plot. These findings suggest that the blocking ETX is located at a site very close to S165 (the external demarcation of the SPM blocking site) with positive membrane voltages or preponderant outward flow. We further explored the possible role

Fig. 5 Inhibition of the E224G and M183N mutant Kir2.1 currents by internal ETX. **a** Sample sweeps demonstrating inhibition of E224G and M183N mutant channels by internal ETX in symmetrical 100 mM K$^+$. Sweeps for each type of mutant channel were recorded with the same protocol as that in Fig. 1 in the absence or presence of internal 1.0 mM ETX. The *dotted lines* indicate the zero current level. **b** The apparent K_d of ETX in the E224G and M183N mutant channels is obtained by the same way as that in Fig. 1b. **c** The K_d values of E224G and M183N mutant channels from **b** are plotted against voltage (the same approach as that in Fig. 1c, $n=5$–8). The *dashed lines* are fits to the data points between −30 and −10 mV (the same approach as that in Fig. 1c), with $K_{d(0)}$ ~25 mM and $Z\delta$ 0.48 (E224G), or $K_{d(0)}$ ~10 mM and $Z\delta$ 0.5 (M183N). The WT channel data (*red line*) are taken from Fig. 1c for comparison
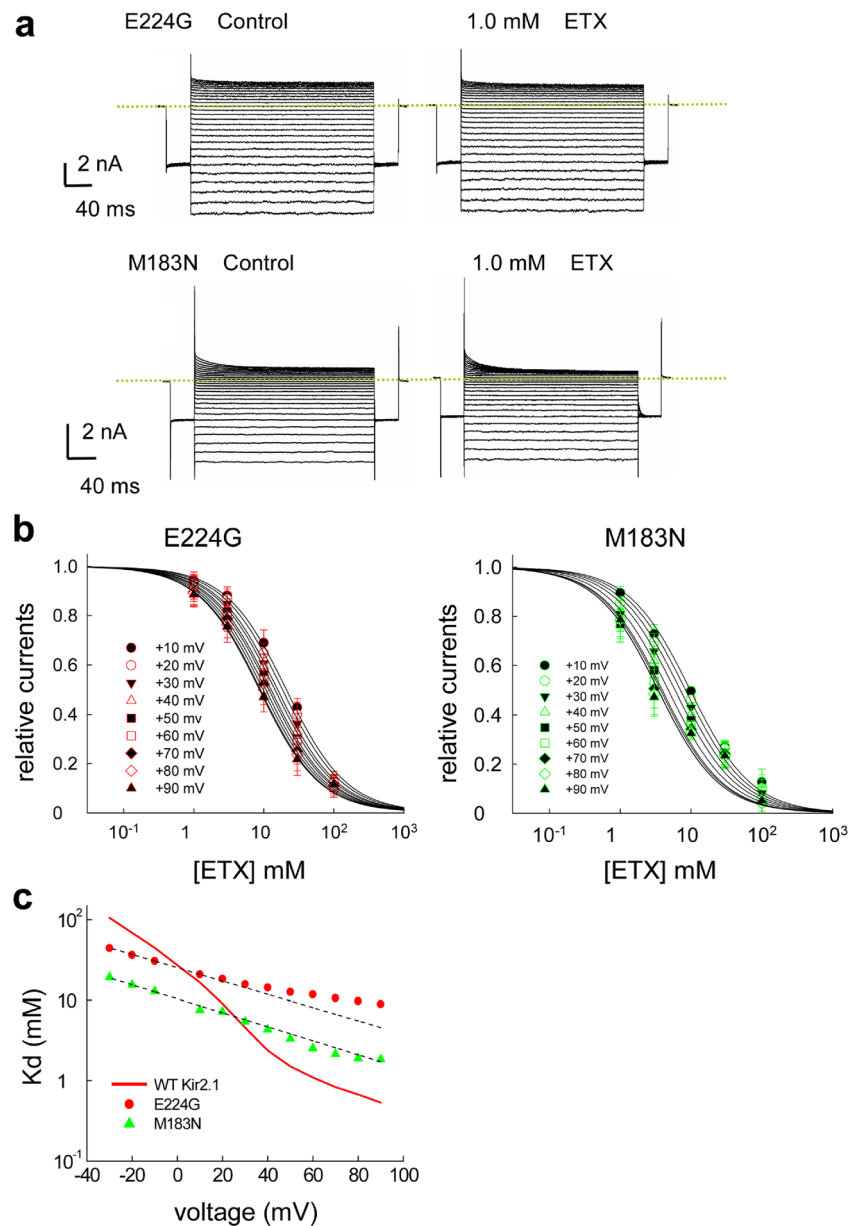

of T141, a residue in close proximity to S165 (Fig. S1). Substitutions with A, E, W, K, and R for T141 yielded only two mutant channels showing enough currents for analysis (T141A and T141E, Fig. S1). Although T141A single mutation does not have an apparently discernible effect on the action of ETX, T141A/S165L double mutation markedly decreases the blocking effect of ETX (Fig. 7a, b). Double mutant cycle analyses of the K_d changes with T141A and S165L mutations reveal a superadditive effect (Fig. 7c). This superadditive effect implies that T141 and especially S165 act as two versatile ligands to accommodate the blocking ETX with outward K$^+$ currents. This idea is substantiated by molecular dynamics simulation, which demonstrates that the –NH group

of ETX may interact with the –OH group in either S165 or T141 (Fig. 8). Moreover, ETX probably does not block the pore simply by itself. Instead, ETX binding to S165 or T141 would induce a dramatic conformation change and narrow the pore at D172 (Figs. 8 and 9).
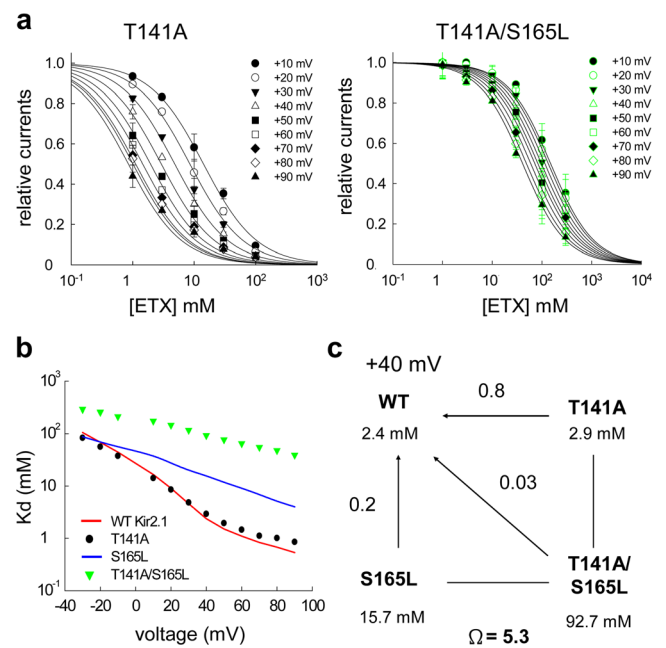
The structural determinants on ETX for the block of Kir2.1 channels

It is interesting that ETX probably binds to residues S165/T141 to induce a pore-narrowing conformational change at D172 to decrease the K$^+$ flow (Fig. 8). It would be desirable to explore the structural determinants on ETX responsible for the induction of this intriguing conformational
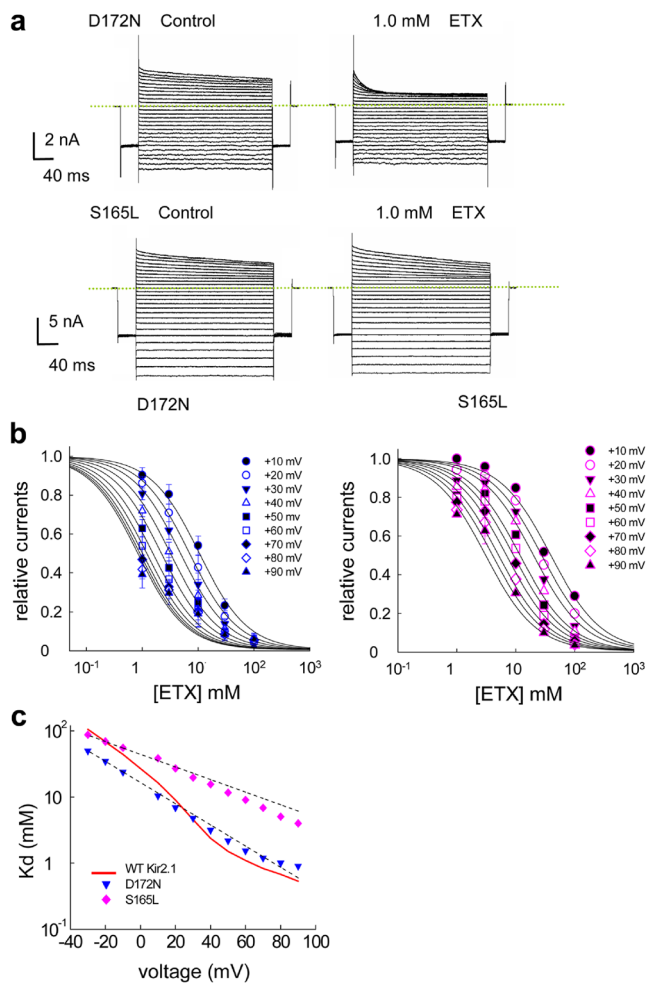
Fig. 6 Inhibition of the D172N and S165L mutant Kir2.1 currents by internal ETX. **a** Sample sweeps demonstrating inhibition of D172N and S165L mutant channels by internal ETX in symmetrical 100 mM K$^+$ (the same protocol as that in Fig. 1). **b** The apparent K_d of ETX in the D172N and S165L mutant channels is obtained by the same way as that in Fig. 1b. **c** The K_d values of D172N and S165L mutant channels from **b** are plotted against voltage (the same approach as that in Fig. 1c, $n=5$–8). The *dashed lines* are fits to the data points between −30 and −10 mV (the same approach as in Fig. 1c), with $K_{d(0)}$ ~16 mM and $Z\delta$ 0.97 (D172N), or $K_{d(0)}$ ~45 mM and $Z\delta$ 0.6 (S165L). The WT channel data (*red line*) are taken from Fig. 1c for comparison


Fig. 7 Inhibition of the T141A and T141A/S165L mutant channels by internal ETX. **a** The apparent K_d of ETX in the T141A and T141A/S165L mutant channels is obtained by the same way as that in Fig. 1b. **b** The K_d values of D172N and S165L mutant channels from **a** are plotted against voltage (the same approach as that in Fig. 1c, $n=5$–8). The *dashed lines* are fits to the data points between −30 and −10 mV (the same approach as that in Fig. 1c), with $K_{d(0)}$ ~25.4 mM and $Z\delta$ 0.99 (T141A), or $K_{d(0)}$ ~190 mM and $Z\delta$ 0.4 (T141A/S165L). The WT channel data (*red line*) are taken from Fig. 1c for comparison. **c** Double-mutant cycle analysis of the T141A + S165L single and double mutant channels at +40 mV. The coupling coefficient (Ω) is defined by the ratio between the product of the K_d changes in each single mutant channel (versus the WT channel) and the K_d changes in the T141A/S165L double mutant channel (versus the WT channel), and is ~5.3 (i.e., $(0.8)\times(0.2)/(0.03)$)

change. Succinimide (SUX) is structurally very similar to ETX but lacks the methyl and ethyl side chains. In concentrations as high as 10 mM, SUX fails to show any discernible effect on the Kir2.1 currents, whether the currents are inward or outward (Fig. 9a). Molecular dynamics simulation shows that –NH group in SUX could also interact with the –OH group in residue T141. However, the orientation of the SUX molecule is different from ETX. The distance between D172 residues therefore remains unchanged with SUX binding (Fig. 9b, c), well consistent with the experimental finding that SUX does not affect Kir2.1 currents. We conclude that the methyl and ethyl side chains play an essential role in the blocking effect of ETX on Kir2.1 channels, possibly via the

induction of changes in the orientation of the peptide chain containing D172, where the pore caliber is then significantly reduced (Fig. 9d).

The superadditive blocking effects of ETX and SPM on the WT Kir2.1 currents

Intracellular SPM is a key blocker and modulator of the WT Kir2.1 channel. Because the SPM binding site in the presence of outward currents involves D172 [10, 17, 46, 47], we studied the possible interaction between ETX and SPM with outward currents. One millimolar ETX and 10 nM SPM were concomitantly applied to the channel of excised inside-out patches (Fig. 10a). There is a superadditive blocking effect in terms of both steady-state and kinetic considerations (Fig. 10b, c), implying the conformational changes induced by ETX sustain in the presence of SPM and facilitate SPM block. This idea is supported by molecular dynamics simulation (Fig. 10d–f). The diagonal distance between D172 residues in the channel pore is similarly reduced to <10 Å by ETX
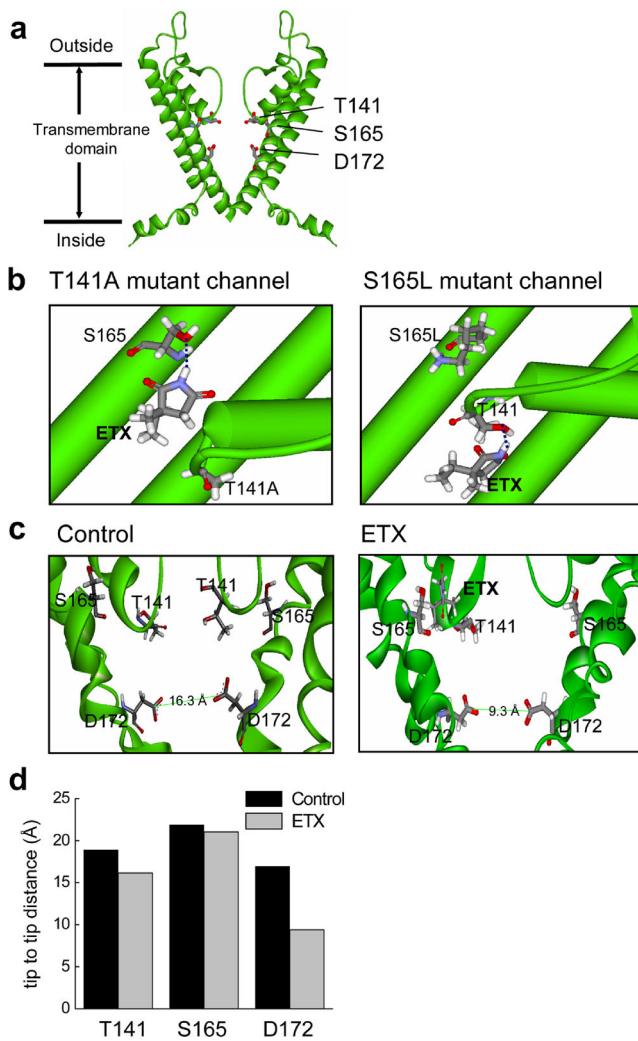
Fig. 8 Molecular dynamics simulation of ETX action in the Kir2.1 channel pore. **a** The homology model is constructed based on the correlative X-ray crystal structures of the mouse Kir2.1 and chicken Kir2.2 channel (see Materials and methods). Side view of the Kir2.1 channel shows the transmembrane domain of the two subunits. **b** In the presence of 40 water molecules and 7 K$^+$ ions, the ETX molecule applied to the cavity region between residues 141 and 165 of the transmembrane domain is found to stay close to the side chains of S165 in the T141A mutant channel (*left panel*). On the other hand, ETX cannot approach S165L but T141 in the S165L mutant channel (*right panel*; stick model: carbon, *grey*; nitrogen, *blue*; hydrogen; *white*; and oxygen, *red*). The –NH group of the ETX molecule may interact with the –OH group at T141 or the –OH group at S165 (*short dashed lines*). **c** The distance between residues D172 from tip to tip is ~16.3 Å in the absence of ETX (*left panel*), but is markedly decreased with ETX binding to either residues S165 or 141 (~9.3 Å, *right panel*). **d** A summary plot of the diagonal (tip–to–tip) distances between residues T141, S165, and D172 in the absence (control) and presence of ETX in the WT Kir2.1 channel

whether SPM is present or not (Fig. 10d–f). ETX thus may synergistically increase the blocking speed and potency of SPM, presumably by narrowing the pore at D172 and consequently prohibiting the outward exit of the blocking SPM and/or decreasing K$^+$ flux across the SPM-blocked region [17].
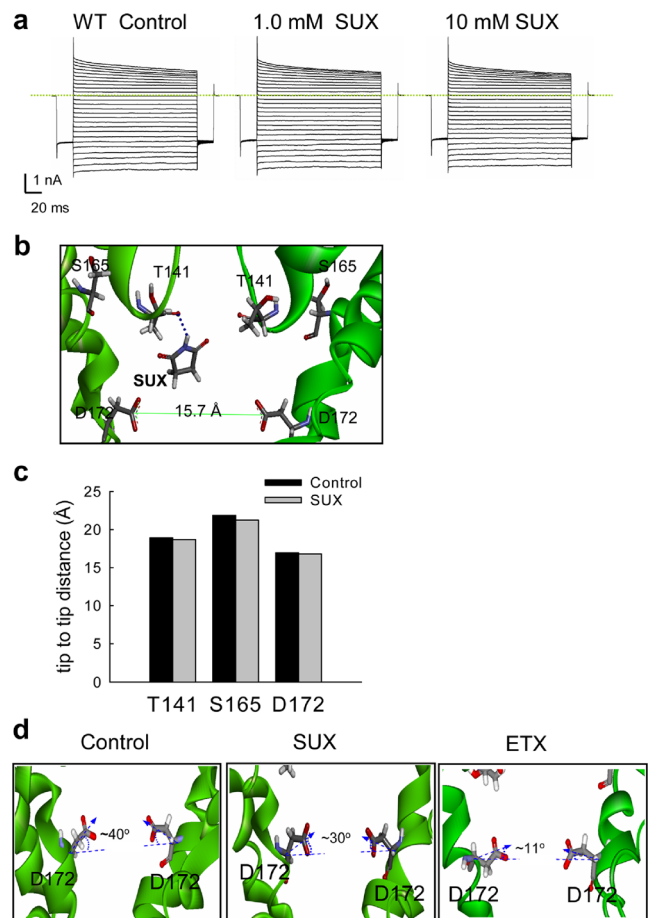
Fig. 9 Lack of a pore-narrowing effect of internal succinimide (SUX). **a** Sample sweeps were recorded in internal 1.0 and 10 mM SUX in WT Kir2.1 channel using the same pulse protocol as that in Fig. 1a. **b** The structure of SUX and possible interactions between SUX and the Kir2.1 channel pore are given by molecular dynamics simulation (the same colors of atoms as that in Fig. 8). With the same approach as that in Fig. 8b, the –NH group of the SUX molecule stay close to the oxygen atom at residue T141 (*short dashed lines*). The tip to tip distance between residues D172, however, remains unchanged by SUX (~15.7 Å). **c** A summary plot of the tip-to-tip diagonal distance between residues T141, S165, and D172 in the absence (control) and presence of SUX in the WT Kir2.1 channel. **d** With the same approach as that in Fig. 8b, ETX has a much more prominent effect of "adducting" D172 side chains to an internally deflected position and thus decreasing the diagonal distance of D172 by ETX but not SUX. The side chains of D172

Discussion

ETX blocks the Kir2.1 channel pore at the external end of the central cavity with outward K$^+$ currents

ETX are uncharged molecules which may freely permeate through cell membrane or relevant lipid-based structure [7, 8]. ETX concentrations in plasma and cerebrospinal fluids (CSF) are thus similar [7]. Also, the mean tissue/plasma ratios of ETX in various brain regions, including cortex, midbrain, cerebellum, and brainstem are fairly close to ~1
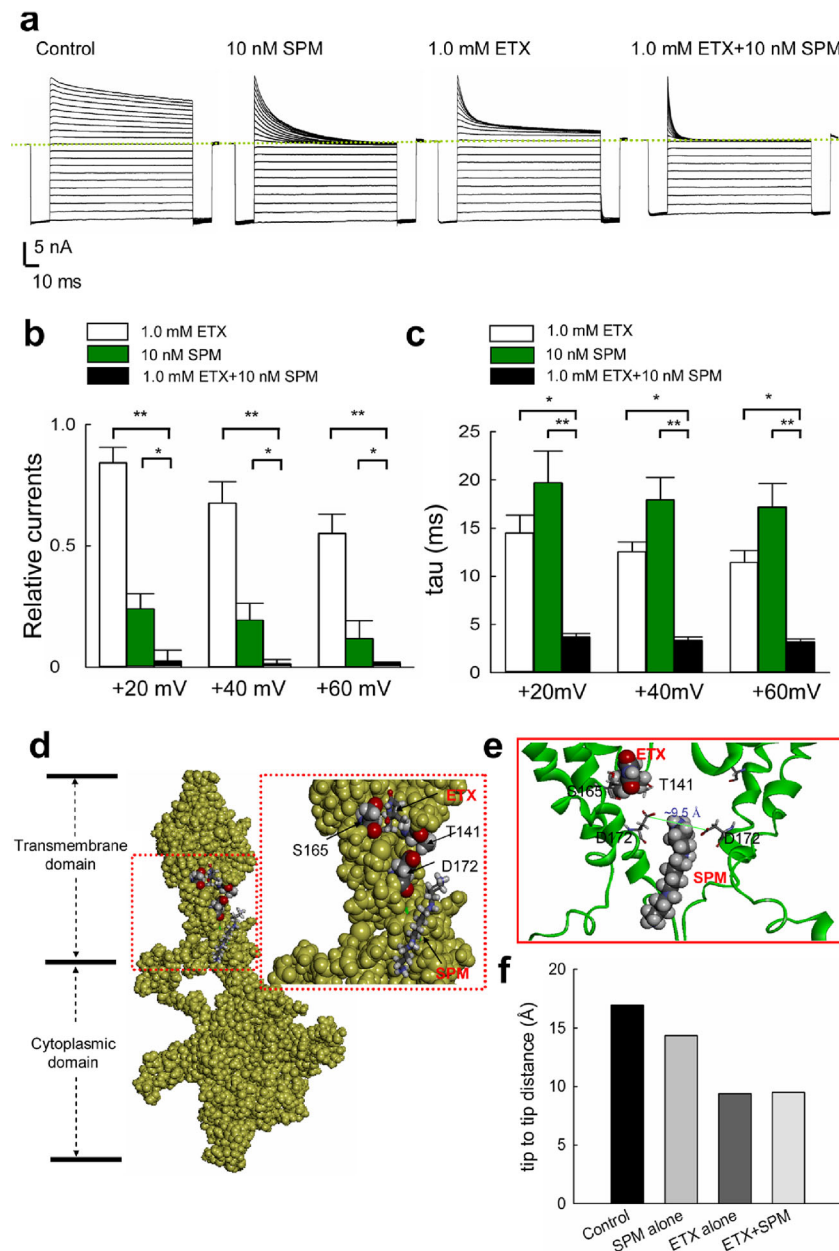
Fig. 10 Superadditive inhibitory effect of concomitant spermine (SPM) and ETX molecules on the WT Kir2.1 channel. **a** Sample sweeps demonstrating the inhibition of WT Kir2.1 currents in the same patch by intracellular 1.0 mM ETX, 10 nM SPM, and combination of 1.0 mM ETX and 10 nM SPM in symmetrical 100 mM K^+. The voltage across the patch membrane was first hyperpolarized from the 0 mV holding potential to −100 mV for 10 ms and then stepped to test voltages from −100 to +100 mV for 150 ms in 10-mV increment. The *dotted lines* indicate the zero current level. **b** Cumulative results were obtained from five patches with the same protocols described in **a**. The relative currents are defined by the ratio between the steady-state WT Kir2.1 currents in 1.0 mM ETX, 10 nM SPM, or concomitant 1.0 mM ETX and 10 nM SPM and that in control. The relative currents (the same definition as that in Fig. 1b, $n=5$) in concomitant 1.0 mM ETX and 10 nM SPM is much smaller than in 1.0 mM ETX or 1.0 nM SPM alone at +20, +40, and +60 mV. *$p<0.05$ and **$p<0.005$, by Student's t test. **c** The decay time constants of the outward currents in the WT channel are much smaller in concomitant

1.0 mM ETX and 10 nM SPM than those in either 1.0 mM ETX or 10 nM SPM. *$p<0.05$ and **$p<0.005$, by Student's t test. **d** In the presence of 40 water molecules, 7 K^+ ions, 1 ETX, and 1 SPM molecules were applied to the central cavity of the Kir2.1 channel. The ETX and SPM molecules of the binding sites are presented in a CPK model (carbon, *grey*; nitrogen, *blue*; and oxygen, *red*). With the same approach as that in Fig. 8b and concomitant application of ETX and SPM, the representative structure of the transmembrane and cytoplasmic domains of one subunit of the WT Kir2.1 channel is presented. A regional view of the residues T141, S165, and D172 in the *boxed panel* (the same colors of atoms as that in Fig. 8). **e** With the same approach as that in **d**, two subunits of the channel are presented in a solid-ribbon model. The distance between diagonal residues D172 from tip to tip is ~9.5 Å in the concomitant presence of ETX and SPM. **e** A summary plot of the tip-to-tip diagonal distance between residues D172 in control, and in the presence of ETX, or SPM, or both in the WT Kir2.1 channel. Note the very similar effect of ETX alone and ETX + SPM

(0.9–0.94) [31]. These results further substantiate that the extracellularly applied ETX could indeed distribute across the cell membrane and exerting its pharmacological effects on the cytoplasmic side. The experimental configuration in this study, e.g., intracellular 0.5–1.0 mM ETX, therefore should be roughly equivalent to the clinical conditions, where ETX would come from the extracellular space (with therapeutic concentrations 0.5–1.0 mM) and equilibrate with the intracellular space of central neurons. We have shown that intracellular ETX has no effect on the inwardly Kir2.1 currents [23] but an evident and dose-dependent inhibitory effect on the outward currents (Fig. 1). ETX therefore seems to block the Kir2.1 channel in a way apparently similar to that of SPM, which is a molecule containing 4 possible charges. Indeed, SPM or ETX in the Kir2.1 channel pore would be pushed to the external end of the flux-coupling region with preponderant outward K^+ currents. However, in contrast to SPM which binds to ~D172 and directly blocks the pore [17, 18], ETX binds to S165 or T141. Moreover, ETX does not seem to have a very specific binding configuration in the vicinity of S165 and T141 (and thus the much larger apparent K_d than SPM) but could block the pore by induction of conformational change at D172 (Figs. 8, 9, 10, and 11). ETX may be chiefly accommodated by S165 in the WT channel. However, if S165 is no longer available (e.g., with S165L mutation), ETX may also be accommodated by T141 (Fig. 8c). S165L/T141A double mutation would make both of the versatile choices impossible and thus markedly decrease the blocking effect of ETX in a superadditive way. In contrast, VPA has no apparent effect on the WT Kir2.1 currents, consistent with the finding that VPA could not form any significant bonds with the Kir2.1 channel pore (Figs. S2 and S3). Also, although the –NH group of SUX forms a hydrogen bond with the oxygen atom in residue T141, no pore-narrowing effect at D172 could be induced (Fig. 9b–d). This is consistent with the lack of discernible effect of SUX on the Kir2.1 currents (Fig. 9a).

The movement of ETX in the flux-coupling region of Kir2.1 channel pore is accompanied by ~1.2 K^+ ions in 100 mM ambient K^+

It is interesting that ETX, presumably an uncharged molecule by itself in physiological conditions, would be capable of moving back and forth in the flux-coupling region of the Kir2.1 channel pore (Fig. 11), showing features of voltage- as well as flow-dependent block. Because the very asymmetrical barrier deduced from the distinct voltage dependence of binding and unbinding kinetics of ETX (Figs. 3 and 4) is also similar to the case of SPM [17], it would be reasonable to assume that the ETX blocking site

in the vicinity of S165/T141 is located at an electrical distance (δ) of ~0.5 from the inside. The $Z\delta$ of the unbinding rate of ETX (0.58, Fig. 4) would then signal that ETX moves in the pore with an equivalent charge of ~1.2. In other words, ETX most likely is accompanied by ~1.2 K^+ ions when traveling in the pore of the Kir2.1 channel in the presence of 100 mM symmetrical K^+ solution. The ~1.2 K^+ seems to be a saturating member as it is unchanged if the ambient K^+ is increased to symmetrical 300 mM K^+. On the other hand, the number of the accompanying K^+ decreases to ~0.9 and ~0.8 in symmetrical 10 and 4 mM K^+, respectively, further substantiating that the movement of ETX is functionally associated with the permeating K^+ from the ambient solution. The associated movement of ETX and permeating K^+ is again reminiscent of the case of SPM. In this regard, it is interesting that the length of each hydrophobic group in SPM is similar to the total length of the ETX molecule (~5.7 Å). This is probably why ETX (with the accompanying K^+) could share some of the Kir2.1 pore-blocking features with SPM. On the other hand, the four charges and three hydrophobic units are connected in a row in SPM, whereas there are at most only ~1.2 charges associated with one hydrophobic unit for the moving ETX in the Kir2.1 channel pore. This could be the reason why there is a much more pronounced rectifying feature of SPM block than ETX. In any case, it is plausible that the flux-coupling region of the Kir2.1 channel pore is composed of regularly or semiregularly spaced hydrophobic and hydrophilic sites and thus is relatively vulnerable to quite a few different blockers from the inside where the entry into the pore is much less censored than those from the outside (as the selectivity filter is located at the external end of the pore).

The modest neuronal depolarization ascribable to Kir2.1 channel block may contribute to the anti-absence effect of ETX

Absence seizures are closely related to the burst mode of discharges of the thalamic relay and especially reticular neurons [3, 13, 41]. The shift between burst (oscillatory) and tonic (relay) modes of discharges in turn is determined by neuronal membrane potential. Depolarization by 2–4 mV may be enough to shift the firing mode from burst to tonic [13, 41]. The clinical therapeutic concentration of ETX reduces burst probability of thalamic reticular nucleus and thalamic relay neurons [26] and increases tonic firing of thalamocortical neurons in slices [20]. According to the findings in Fig. 2, 1 mM ETX (a high therapeutic concentration of ETX) could inhibit ~10 % of the outward K^+ currents through the Kir2.1 channel at −50
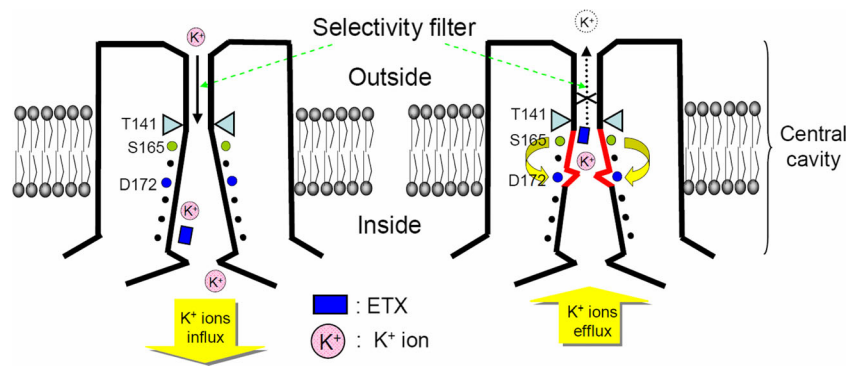
Fig. 11 A schematic model describing the intracellular ETX blocking effect on the Kir2.1 channel. The blocking ETX in the flux-coupling segment can take different positions according to the K^+ flux. When there are outward K^+ currents (preponderant K^+ efflux in the segment), ETX is "pushed" to the most external position of the flux-coupling segment and interacts with S165 or T141 just internal to the selectivity filter of the pore. Conformational changes are then induced at ~D172, where marked pore narrowing happens to decrease K^+ flux. When there are inward K^+ currents (preponderant K^+ influx in the segment), ETX would take the innermost position in the relatively wide part of the flux-coupling segment, inducing no pore narrowing, and thus only a partial or less pronounced block of the K^+ currents. The blocking ETX at this innermost position would need to cross the energy barrier at the inner end of the bundle-crossing region to exit the flux-coupling segment, and the pore is then completely unblocked. This is why there is an initial fast phase followed by a slow phase (slow tail) in the development of the inward currents upon membrane hyperpolarization following a depolarizing pulse in the presence of internal ETX

to −70 mV in physiology conditions (presumably 4 mM external and 140 mM internal K^+). Based on the Goldman–Hodgkin–Katz equation, P_K^+/P_{Na}^+ in the cell membrane is simplistically ~16/1 (in intracellular K^+, intracellular Na^+, extracellular K^+, and extracellular Na^+: 140, 10, 4, and 140 mM, respectively) to make a resting membrane potential of −60 mV assuming no other coexisting major conductance. If the major K^+ conductances in the resting condition are as ascribed to the inward rectifier K^+ channels, a 10 % reduction of P_K^+ by 1 mM ETX may then depolarize the neuron by ~2 mV. A depolarization effect by ~2 mV might be hard to document convincingly in thalamic neurons, which usually do not have a stable resting membrane potential especially when finding in the burst mode. However, with a slope factor of ~7.3 for the inactivation curve of T-type Ca^{2+} channels (in thalamic neurons [25]), a ~2 mV depolarization in membrane potential in the vicinity of V_{half} (where ~50 % of the channel is available) would decrease the channel availability from ~50 to ~43 %, or a ~14 % decrease in the available T-type Ca^{2+} currents. This modest decrease in T-type Ca^{2+} currents presumably would have a significant effect only on those neurons with a borderline amount of available T-type Ca^{2+} currents, switching their firings from the burst mode to the tonic mode of discharge. This could be consistent with the finding that ETX not only reduces burst probability of thalamic neurons [26] but also increase tonic firings of thalamocortical neurons in slice [20]. One way to envisage the pharmacological effect of ETX against absence seizures thus could be a depolarizing effect too modest to be reliably and directly measured, but enough to decrease the availability of T-type Ca^{2+} channels, as well as thalamic burst discharges, and enough

to slightly increase the "excitability" of the thalamic neurons for tonic discharges [13, 20, 25]. The modest effect of ETX on membrane potential and T-type Ca^{2+} currents could actually be the key attribute making ETX a clinically useful regimen against absence seizures, as ETX could then have a relatively "selective" inhibition of those abnormally enhanced bursts which happen to rely on a modest increase of available T-type Ca^{2+}. ETX may therefore have only minimal cognitive side effects [11], and if adverse reactions of ETX do happen, the common ones are those associated with the inappropriately suppressed burst discharges in the thalamocortical and/or vestibulocerebellar circuits (e.g., decrease in concentration, sleep disorder, and dizziness) [11]. In summary, the modest inhibition of inward rectifier K^+ currents by ~1.0 mM ETX could reasonably contribute to the anti-absence effect of ETX. It may work together with direct inhibition of persistent Na^+ currents [5, 26] and/or T-type Ca^{2+} currents [4, 24] to decrease burst discharges and thus absence seizures. It would be desirable to investigate if the different clinical effect between ETX and VPA could be at least partly ascribable to the different effect on the Kir2.1 currents and if ETX has the other clinical applications in view of the growing list of neuropsychiatric functions and dysfunctions associated with inward rectifier K^+ currents.

References

1. Berendsen HJC, Postma JPM, Vangunsteren WF, Dinola A, Haak JR (1984) Molecular-dynamics with coupling to an external bath. J Chem Phys 81:3684–3690

2. Chakraborty AT, Youssef I (2009) Successful treatment of intractable post-ictal psychosis with adjunctive ethosuximide. Seizure 18(1):84. doi:10.1016/j.seizure.2008.08.006

3. Cheong E, Shin HS (2013) T-type Ca(2)(+) channels in absence epilepsy. Biochim Biophys Acta 1828(7):1560–1571. doi:10.1016/j.bbamem.2013.02.002

4. Coulter DA, Huguenard JR, Prince DA (1989) Specific petit mal anticonvulsants reduce calcium currents in thalamic neurons. Neurosci Lett 98(1):74–78

5. Crunelli V, Leresche N (2002) Block of thalamic T-Type Ca(2+) channels by ethosuximide is not the whole story. Epilepsy Curr 2(2):53–56. doi:10.1046/j.1535-7597.2002.00024.x

6. Crunelli V, Leresche N (2002) Childhood absence epilepsy: genes, channels, neurons and networks. Nat Rev Neurosci 3(5):371–382. doi:10.1038/nrn811

7. Eriksson AS, Hoppu K, Nergardh A, Boreus L (1996) Pharmacokinetic interactions between lamotrigine and other antiepileptic drugs in children with intractable epilepsy. Epilepsia 37(8):769–773

8. Ferrendelli JA, Kinscherf DA (1979) Inhibitory effects of anticonvulsant drugs on cyclic nucleotide accumulation in brain. Ann Neurol 5(6):533–538. doi:10.1002/ana.410050606

9. Fujiwara Y, Kubo Y (2002) Ser165 in the second transmembrane region of the Kir2.1 channel determines its susceptibility to blockade by intracellular Mg2+. J Gen Physiol 120(5):677–693

10. Fujiwara Y, Kubo Y (2006) Functional roles of charged amino acid residues on the wall of the cytoplasmic pore of Kir2.1. J Gen Physiol 127(4):401–419

11. Glauser TA, Cnaan A, Shinnar S, Hirtz DG, Dlugos D, Masur D, Clark PO, Capparelli EV, Adamson PC (2010) Ethosuximide, valproic acid, and lamotrigine in childhood absence epilepsy. N Engl J Med 362(9):790–799. doi:10.1056/NEJMoa0902014

12. Goren MZ, Onat F (2007) Ethosuximide: from bench to bedside. CNS Drug Rev 13(2):224–239

13. Gorji A, Mittag C, Shahabi P, Seidenbecher T, Pape HC (2011) Seizure-related activity of intralaminar thalamic neurons in a genetic model of absence epilepsy. Neurobiol Dis 43(1):266–274. doi:10.1016/j.nbd.2011.03.019

14. Hansen SB, Tao X, MacKinnon R (2011) Structural basis of PIP2 activation of the classical inward rectifier K + channel Kir2.2. Nature 477(7365):495–498. doi:10.1038/nature10370

15. Hille B (2001) Ionic channels of excitable membrane. Sinauer assoc, Sunerland MA

16. Howe MW, Feig SL, Osting SM, Haberly LB (2008) Cellular and subcellular localization of Kir2.1 subunits in neurons and glia in piriform cortex with implications for K + spatial buffering. J Comp Neurol 506(5):877–893. doi:10.1002/cne.21534

17. Huang CW, Kuo CC (2014) The bundle crossing region is responsible for the inwardly rectifying internal spermine block of the Kir2.1 channel. Pflugers Arch 466(2):275–293. doi:10.1007/s00424-013-1322-0

18. Huang CW, Kuo CC (2014) Gating of the Kir2.1 channel at the bundle crossing region by intracellular spermine and other cations. J Cell Physiol. doi:10.1002/jcp.24616

19. Hughes JR (2009) Absence seizures: a review of recent reports with new concepts. Epilepsy Behav 15(4):404–412. doi:10.1016/j.yebeh.2009.06.007

20. Huguenard JR, Prince DA (1994) Intrathalamic rhythmicity studied in vitro: nominal T-current modulation causes robust antioscillatory effects. J Neurosci 14(9):5485–5502

21. Karschin C, Dissmann E, Stuhmer W, Karschin A (1996) IRK(1-3) and GIRK(1-4) inwardly rectifying K + channel mRNAs are differentially expressed in the adult rat brain. J Neurosci 16(11):3559–3570

22. Kim D, Song I, Keum S, Lee T, Jeong MJ, Kim SS, McEnery MW, Shin HS (2001) Lack of the burst firing of thalamocortical relay neurons and resistance to absence seizures in mice lacking alpha (1G) T-type Ca(2+) channels. Neuron 31(1):35–45

23. Kobayashi T, Hirai H, Iino M, Fuse I, Mitsumura K, Washiyama K, Kasai S, Ikeda K (2009) Inhibitory effects of the antiepileptic drug ethosuximide on G protein-activated inwardly rectifying K + channels. Neuropharmacology 56(2):499–506. doi:10.1016/j.neuropharm.2008.10.003

24. Kostyuk PG, Molokanova EA, Pronchuk NF, Savchenko AN, Verkhratsky AN (1992) Different action of ethosuximide on low- and high-threshold calcium currents in rat sensory neurons. Neuroscience 51(4):755–758

25. Kuo CC, Yang S (2001) Recovery from inactivation of T-type Ca2+ channels in rat thalamic neurons. J Neurosci 21(6):1884–1892

26. Leresche N, Parri HR, Erdemli G, Guyon A, Turner JP, Williams SR, Asprodini E, Crunelli V (1998) On the action of the anti-absence drug ethosuximide in the rat and cat thalamus. J Neurosci 18(13):4842–4853

27. Lou KL, Huang PT, Shiau YS, Liaw YC, Shiau YY, Liou HH (2003) A possible molecular mechanism of hanatoxin binding-modified gating in voltage-gated K + -channels. J Mol Recognit 16(6):392–395. doi:10.1002/jmr.614

28. Miyashita T, Kubo Y (1997) Localization and developmental changes of the expression of two inward rectifying K(+)-channel proteins in the rat brain. Brain Res 750(1–2):251–263

29. Nagao Y, Harada Y, Mukai T, Shimizu S, Okuda A, Fujimoto M, Ono A, Sakagami Y, Ohno Y (2013) Expressional analysis of the astrocytic Kir4.1 channel in a pilocarpine-induced temporal lobe epilepsy model. Front Cell Neurosci 7:104. doi:10.3389/fncel.2013.00104

30. Neusch C, Weishaupt JH, Bahr M (2003) Kir channels in the CNS: emerging new roles and implications for neurological diseases. Cell Tissue Res 311(2):131–138. doi:10.1007/s00441-002-0669-x

31. Patel IH, Levy RH, Rapport RL (1977) Distribution characteristics of ethosuximide in discrete areas of rat brain. Epilepsia 18(4):533–541

32. Pegan S, Arrabit C, Zhou W, Kwiatkowski W, Collins A, Slesinger PA, Choe S (2005) Cytoplasmic domain structures of Kir2.1 and Kir3.1 show sites for modulating gating and rectification. Nat Neurosci 8(3):279–287

33. Posner EB, Mohamed K, Marson AG (2005) Ethosuximide, sodium valproate or lamotrigine for absence seizures in children and adolescents. Cochrane Database Syst Rev 4, CD003032. doi:10.1002/14651858.CD003032.pub2

34. Pruss H, Derst C, Lommel R, Veh RW (2005) Differential distribution of individual subunits of strongly inwardly rectifying potassium channels (Kir2 family) in rat brain. Brain Res Mol Brain Res 139(1):63–79. doi:10.1016/j.molbrainres.2005.05.006

35. Rodriguez-Menchaca AA, Navarro-Polanco RA, Ferrer-Villada T, Rupp J, Sachse FB, Tristani-Firouzi M, Sanchez-Chapula JA (2008) The molecular basis of chloroquine block of the inward rectifier Kir2.1 channel. Proc Natl Acad Sci U S A 105(4):1364–1368. doi:10.1073/pnas.0708153105

36. Salke-Kellermann RA, May T, Boenik HE (1997) Influence of ethosuximide on valproic acid serum concentrations. Epilepsy Res 26(2):345–349

37. Sarkisova KY, Kuznetsova GD, Kulikov MA, van Luijtelaar G (2010) Spike-wave discharges are necessary for the expression of behavioral depression-like symptoms. Epilepsia 51(1):146–160. doi:10.1111/j.1528-1167.2009.02260.x

38. Sayer RJ, Brown AM, Schwindt PC, Crill WE (1993) Calcium currents in acutely isolated human neocortical neurons. J Neurophysiol 69(5):1596–1606

39. Shaw FZ, Chuang SH, Shieh KR, Wang YJ (2009) Depression- and anxiety-like behaviors of a rat model with absence epileptic discharges. Neuroscience 160(2):382–393. doi:10.1016/j.neuroscience.2009.02.053

40. Shiau YS, Huang PT, Liou HH, Liaw YC, Shiau YY, Lou KL (2003) Structural basis of binding and inhibition of novel tarantula toxins in mammalian voltage-dependent potassium channels. Chem Res Toxicol 16(10):1217–1225. doi:10.1021/tx0341097

41. Slaght SJ, Leresche N, Deniau JM, Crunelli V, Charpier S (2002) Activity of thalamic reticular neurons during spontaneous genetically determined spike and wave discharges. J Neurosci 22(6):2323–2334

42. Steinhauser C, Seifert G (2002) Glial membrane channels and receptors in epilepsy: impact for generation and spread of seizure activity. Eur J Pharmacol 447(2–3):227–237

43. Tao X, Avalos JL, Chen J, MacKinnon R (2009) Crystal structure of the eukaryotic strong inward-rectifier K + channel Kir2.2 at 3.1 A resolution. Science 326(5960):1668–1674

44. Thompson SM, Wong RK (1991) Development of calcium current subtypes in isolated rat hippocampal pyramidal cells. J Physiol 439:671–689

45. Vrielynck P (2013) Current and emerging treatments for absence seizures in young patients. Neuropsychiatr Dis Treat 9:963–975. doi:10.2147/NDT.S30991

46. Xie LH, John SA, Weiss JN (2002) Spermine block of the strong inward rectifier potassium channel Kir2.1: dual roles of surface charge screening and pore block. J Gen Physiol 120(1):53–66

47. Xie LH, John SA, Weiss JN (2003) Inward rectification by polyamines in mouse Kir2.1 channels: synergy between blocking components. J Physiol 550(Pt 1):67–82. doi:10.1113/jphysiol.2003.043117

48. Yamada K, Ji JJ, Yuan H, Miki T, Sato S, Horimoto N, Shimizu T, Seino S, Inagaki N (2001) Protective role of ATP-sensitive potassium channels in hypoxia-induced generalized seizure. Science 292(5521):1543–1546. doi:10.1126/science.1059829

49. Yamada A, Uesaka N, Hayano Y, Tabata T, Kano M, Yamamoto N (2010) Role of pre- and postsynaptic activity in thalamocortical axon branching. Proc Natl Acad Sci U S A 107(16):7562–7567. doi:10.1073/pnas.0900613107